JOURNAL OF SYNCHROTRON RADIATION

ISSN 1600-5775

Received 15 July 2015
Accepted 1 October 2015

Edited by M. Zangrando, Elettra and IOM-CNR, Italy

Keywords: filamentation; X-ray; FEL; attenuation; gas; photoabsorption; diffusion.

Filamentation effect in a gas attenuator for high-repetition-rate X-ray FELs

Yiping Feng,* Jacek Krzywinski, Donald W. Schafer, Eliazar Ortiz, Michael Rowen and Tor O. Raubenheimer

Linac Coherent Light Source, SLAC National Accelerator Laboratory, 2575 Sand Hill Road, Menlo Park, CA 94025, USA. *Correspondence e-mail: yfeng@slac.stanford.edu

A sustained filamentation or density depression phenomenon in an argon gas attenuator servicing a high-repetition femtosecond X-ray free-electron laser has been studied using a finite-difference method applied to the thermal diffusion equation for an ideal gas. A steady-state solution was obtained by assuming continuous-wave input of an equivalent time-averaged beam power and that the pressure of the entire gas volume has reached equilibrium. Both radial and axial temperature/density gradients were found and describable as filamentation or density depression previously reported for a femtosecond optical laser of similar attributes. The effect exhibits complex dependence on the input power, the desired attenuation, and the geometries of the beam and the attenuator. Time-dependent simulations were carried out to further elucidate the evolution of the temperature/density gradients in between pulses, from which the actual attenuation received by any given pulse can be properly calculated.

1. Introduction

In the last decade, short-wavelength free-electron lasers (FELs) based on both self-amplified spontaneous emission (SASE) and seeding schemes have been constructed, commissioned and put into user operation (Ackermann *et al.*, 2007; Emma *et al.*, 2010; Ishikawa *et al.*, 2012; Allaria *et al.*, 2012). The extraordinary properties of the FEL radiation including the ultrashort duration, unprecedented peak brightness and fully transverse coherence have enabled and are continuing to enable scientists to push the very boundaries of their scientific pursuits and make important discoveries in physics, chemistry, biology, material and energy sciences. To best facilitate and maximize the scientific output of the user measurements, various diagnostic, optical and beam manipulation devices specifically designed for working with FEL beams are required. A FEL attenuator is such a device for reducing the energy of the FEL pulses in a controlled manner before their delivery to the experimental apparatus. For example, when aligning an X-ray detector the full FEL beam is applied only when the scattered intensity onto the detector is confirmed to be within the safe limit. Using an attenuated beam and gradually increasing the pulse energy is a common experimental practice, and a very important one. The FEL attenuator must not only withstand the extremely high peak fluence of the FEL beam but also dissipate the absorbed energy sufficiently quickly before the arrival of subsequent pulses. The former requirement is used to down-select techniques that can be employed to build such a device, and for attenuating a soft X-ray FEL beam a gas medium must be

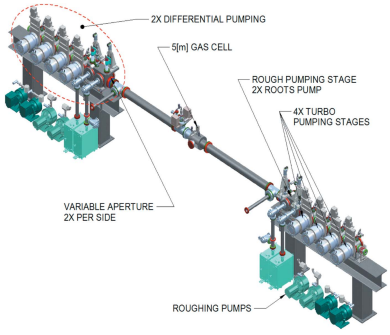

used; this has been implemented at various facilities including the Free electron LASer at Hamburg (FLASH) VUV FEL (Hahn & Tiedtke, 2007) and the Linac Coherent Light Source (LCLS) X-ray FEL (Ryutov *et al.*, 2009).

A typical gas attenuator consists of a many meters long windowless gas tube filled with a gas of choice, such as N_2 or argon, with its pressure regulated and adjusted for varying the degree of attenuation. The gas tube is book-ended by long differential pumping sections for maintaining ultrahigh vacuum conditions elsewhere. The quick recovery requirement has not received much attention and has always been assumed to be satisfied as in the case of the gas attenuator built for the LCLS X-ray FEL operating at a maximum repetition rate of 120 Hz. There the inter-pulse duration of 8.3 ms is thought to be sufficiently long such that the physical attributes of the gas volume return to the original values, including most importantly the effective density probed by the X-rays, before the arrival of the next pulse. The total average power dissipation is of the order of a fraction of a Watt for an average pulse energy of $\sim$2 mJ and any appreciable attenuation factor (>2). There is a direct and predictable correspondence between the gas pressure and the prescribed attenuation, which can be simply calculated based on the total mass attenuation coefficient of the gas species, density and effective length of the X-ray–gas interaction region.

The situation will likely be significantly different for attenuating the high-repetition-rate FEL beams produced by the future LCLS-II soft and hard X-ray undulators, which are fed by a 4 GeV superconducting radiofrequency (SCRF) accelerator, or high-repetition-rate pulse trains from the future European XFEL. Both the LCLS-II soft (200 to 1300 eV) and hard X-ray (1 to 5 keV) SCRF FELs are being designed to operate up to 1 MHz in the continuous-wave mode and to generate pulses with maximum energy of a few mJ. The maximum average FEL power, however, will be capped at 200 W by a combination of reducing the frequency and/or using lower electron bunch charge to produce lower per-pulse energy. The baseline design for the LCLS-II gas attenuator (Schafer, 2015) will be of the same concept as that of LCLS (Ryutov *et al.*, 2009), consisting of a 5 m-long gas tube filled with argon with a maximum operating pressure of 7 Torr, as shown in Fig. 1. At the maximum operating repetition rate of 1 MHz, the short inter-pulse duration of 1 µs is presumed to be insufficient for the entire gas volume to relax completely back to its starting conditions. Consequently, there will be a transient where trailing pulses will likely 'see' a higher temperature and thus lower density condition because of the heating effect by the absorbed energy. The actual attenuation will be lower and will depend on the prior history of energy deposition and thermal relaxation in the system and cannot be predetermined by a simple calculation using the equilibrium gas pressure alone, as opposed to how it is done for the current LCLS attenuator.

This 'gas filamentation' phenomenon has been previously reported in an experiment using ultrashort optical lasers by Cheng *et al.* (2013). They observed a lower-density filament induced in a 1 atm N_2 gas cell that was irradiated by 800 nm 40 fs-long Ti:sapphire laser pulses with a beam diameter of 100 µm, an average energy of 0.72 mJ pulse^{-1}, and operating at a repetition rate of 20 Hz. The density depression in the filament was as high as 20% and the recovery time was $\sim$1 ms, as measured using an interferometric technique after a single pulse. There, a low laser repetition rate of 20 Hz was used to isolate and observe the single pulse effect. The basic mechanism of the 'gas filamentation' effect is the energy deposition in the gas, which causes the gas to heat up and expand, and the thermal conductivity of the gas is finite so the dissipation of the extra energy takes place over a finite time. We believe that a similar density depression phenomenon is likely to exist in the FEL gas attenuator because a similar magnitude of per-pulse energy of a few mJ will be absorbed, although the exact energy deposition mechanism and profile will be somewhat different. In this report, we present thermodynamic studies using 'finite-difference methods' to simulate both the steady state and transient temperature and density distributions in the LCLS-II attenuator under high-repetition-rate operation, revealing the same 'gas filamentation' effect in the limit of not a single pulse but a continuous pulse train. Its magnitude has complex dependences on many parameters, including the average input power, desired attenuation (thus the absorbed power), pulse structure, geometries of both the beam and pipe, and gas properties including thermodiffusivity, and mass attenuation coefficient. As such, the achieved attenuation is significantly different than expected for a low-repetition operation, and cannot be easily predetermined. It must be measured and tabulated as a lookup table for subsequent requests, presenting operational challenges and requiring additional confirmation by downstream energy measurement devices.

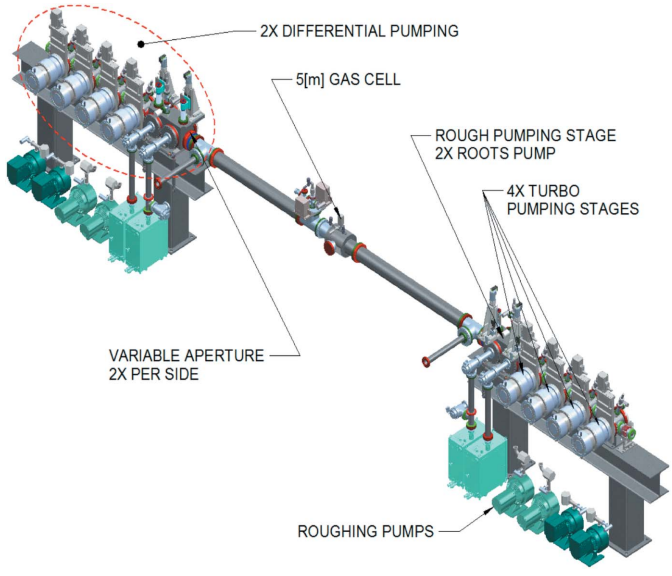

Figure 1
Mechanical rendering of the LCLS-II soft X-ray gas attenuator, consisting of a 5 m-long and 150 mm-diameter windowless gas tube filled with argon gas operating at a maximum pressure of 7 Torr, and differential pumping stages on both ends for maintaining an ultrahigh vacuum environment elsewhere.

2. Thermodynamic simulation of density depression

The interactions between the femtosecond X-ray FEL pulses and gas molecules in the attenuator are very complex and different from those by an optical laser discussed by Cheng *et al.* (2013), but they are not the focus of this report. For the purpose of our thermodynamic simulations, it is suffice to assume that, after the initial photoionization of a small percentage of the molecules, many fast electronic processes including Auger decay, inelastic collisions, impact ionization, attachment, recombination, *etc.* would first help thermalize the energy of the primary electrons into the thermal energy of all free electrons (primary and secondary), ions and other excited molecular species. This thermalization process should be complete on a time scale of a few to tens of picoseconds. According to Cheng *et al.* (2013), what follows on a time scale of a few to tens of nanoseconds is the repartitioning of the energy in the electronic/ionic/molecular excitations degrees of freedom into an essentially fully recombined gas in its ground electronic state. The result of the repartitioning will create a temperature gradient, which in turn creates a pressure gradient since the local (by now fully recombined) gas density remains more or less unchanged on time scales shorter than a few nanoseconds. Given the gas attenuator's large ratio of length over radius to be described below, both the temperature and pressure gradients are largest in the radial direction. This pressure gradient will drive hydrodynamic motion of the gas in the form of density (hydrodynamic) waves on a time scale of tens of nanoseconds to a few microseconds to eventually establish constant pressure radially, after the hydrodynamic motion (macroscopic fluid velocity $v \simeq 0$) of the gas molecules arising from the pressure gradient all but ceased. At the end of the pressure equilibration, quasi-equilibrium is reached where the temperature gradient remains largely unchanged, but a density profile or depression develops over the same length scale set by the temperature gradient. Further evolution of the gas in temperature and density will be thermal diffusion dominated on time scales ranging from a few microseconds to a few milliseconds or even longer, and is the focus of the present simulation studies to understand the effect that the density depression created by the proceeding pulses would have on subsequent pulses in terms of the achieved attenuation and associated uncertainties, if the deposited energy fluctuates as in the case of most X-ray FEL lasers.

Two separate but related thermodynamic simulations were performed, one assuming the gas has reached a steady-state equilibrium distribution under a constant continuous-wave (CW) input power, and the other aimed to elucidate the time-dependent aspect of density and temperature gradients in between the pulses, from which the actual attenuation for any given pulse can be evaluated. The first case represents the asymptotic solution ($t \rightarrow \infty$) of the second case when the repetition rate of the FEL approaches infinity while the per-pulse energy becomes infinitesimally small but the total input power is kept constant. The gas attenuator was idealized as shown in Fig. 2 to be a 5 m-long and 20 mm-diameter tube

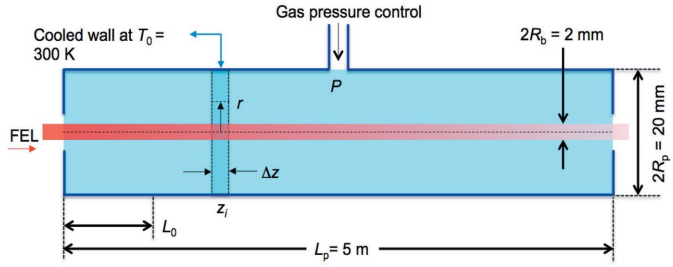

Figure 2
The geometric model of a cylindrical gas attenuator used for the thermodynamic simulation. The attenuator is 5 m in effective total length and 20 mm in diameter and filled with argon gas. The walls of the attenuator are cooled and kept at a constant temperature $T_0 = 300$ K. The X-ray FEL beam of diameter 2 mm with a flat-top transverse profile enters from the left.

filled with argon gas regulated to equilibrium pressure P and irradiated by a 200 eV soft X-ray FEL beam of 2 mm diameter. The FEL pulses are 50 fs long and have per-pulse energy of 2 mJ, and operate at a repetition rate of 100 kHz, producing an average beam power of 200 W. The walls of the gas tube are cooled and kept at a constant temperature of $T_0 =$ 300 K. Based on discussions above, we further assume that the thermalization ($\leq$ a few ps), repartitioning ($\leq$ a few ns) and pressure equilibration ($\leq$ a few μs) processes are all spatially confined to the region of the initial energy deposition which can be considered as instantaneous and is given simply by the transverse profile of the X-ray FEL beam. In the pressure range the gas attenuator will be operating in and on time scales longer than pressure equilibration, the argon gas can be treated as ideal and local temperature $T(r, t)$ and density $n(r, t)$ are well defined variables that always conform to the relation $n(r, t)T(r, t) = n_0T_0 = P/k_B$, where T_0 and n_0 are the background temperature and density at an equilibrium pressure P.

2.1. The steady-state solution for CW input of constant power

Here we first look at the case when the pulse structure of the FEL is replaced by a CW input of equivalent average power and after the gas has reached a steady-state condition that the local temperature and density are no longer changing in time, *i.e.* $T(r, t) = T(r)$, and $n(r, t) = n(r)$, and the relation $n(r)T(r) = n_0T_0 = P/k_B$ still holds. The Fourier law for heat transfer is utilized in solving the equilibrium temperature distribution $T(r)$ and by assuming the energy deposition is limited to within the footprint of the beam only. The problem can be further simplified by two additional assumptions: (*a*) the transverse beam profile is of a flat-top shape with an integrated intensity equivalent to that of the actual Gaussian-like beam; (*b*) heat transfer is absent in the azimuthal direction due to symmetry, but is predominantly in the radial direction and negligible in the axial direction because of the 500:1 length-over-radius ratio.

Based on assumption (*b*), the numerical simulation was performed by dividing the gas volume into thin disks of thickness Δz as depicted in Fig. 2, and solving essentially a

one-dimensional partial differential equation for $T(r, z)$ in variable r only in cylindrical coordinates starting from the center and beginning of the gas cell. The temperature profile was solved sequentially for each (ith) disk starting from the first disk at $z_i = 0$ with boundary conditions at the wall ($r = R_p$) for temperature and the amount of heat generation derived based on the temperature profiles of all proceeding disks ($z < z_i$). By recognizing that outside of the energy deposition profile ($r > R_b$) the heat generation is constant, the integral form of the Fourier law for the ith disk becomes

$$-\kappa 2\pi r \Delta z \frac{\partial T(r, z_i)}{\partial r} = \int_0^{R_b}\int_0^{2\pi} I(r, z_i)\left\{1 - \exp\left[-\frac{T_0 P}{T(r, z_i) P_0 L_0}\Delta z\right]\right\} r\, dr\, d\varphi, \quad (1)$$

where the left-hand side (LHS) represents the surface integral of the heat flux and right-hand side (RHS) is the amount of incremental heat generation within Δz at z_i. More specifically, $\kappa = \kappa_0\sqrt{T}/\sqrt{T_0}$ is the temperature-dependent thermal conductivity of the (ideal) gas referenced to κ_0 at a reference temperature chosen for convenience as the constant temperature T_0, L_0 is the attenuation length of the gas at reference temperature T_0 and reference pressure P_{ref}, $P(0)$ is the starting equilibrium pressure in the low power limit and $I(r, z_i)$ is the intensity profile of the FEL beam at z_i. An approximation can be made to the RHS by using $T(R_b, z_i)$ rather than the actual temperature profile for $r < R_b$ to avoid solving a very complex differential-integral equation, and, by defining $Q(z_i) = 2\pi \int_0^{R_b} I(r, z_i) r\, dr$ as the power at z_i and recognizing $Q(0)$ as simply the input CW power, equation (1) then becomes, after integration in r,

$$\kappa_0 \frac{4\pi}{3\sqrt{T_0}}\left[T(r, z_i)^{3/2} - T_0^{3/2}\right] = Q(z_i)\frac{T_0 P(0)}{T(R_b, z_i) P_{ref} L_0}\ln\left(\frac{R_p}{r}\right). \quad (2)$$

Equation (2) is first solved iteratively for $T(R_b, z_i)$ at R_b, which was then used for obtaining $T(r, z_i)$ for $r > R_b$. The temperature profile for $r < R_b$ was then computed in multiple steps from the edge of the beam inward using a similar relation to equation (1) with the upper limit of the integration in r modified accordingly, and again using a constant temperature obtained in the previous step in evaluating the RHS. Only after $T(r, z_i)$ was solved could the intensity profile $I(r, z_{i+1})$ for the $i + 1$th disk then be calculated and used for solving the temperature profile $T(r, z_{i+1})$. The actual achieved attenuation $\mu[Q(0)]$ was simply given by the power at $z = L_p$ by integrating the intensity profile $I(r, L_p)$.

As the CW input power $Q(0) \to 0$, the achieved attenuation $\mu(0)$ is expected to approach that calculated simply by using the equilibrium pressure in the low power limit. As the power increases, the actual achieved attenuation $\mu[Q(0)]$ will be reduced and the pressure must be increased. The entire computational sequence was then repeated iteratively by adjusting the equilibrium pressure from the low power limit $P(0)$ to an eventual value $P[Q(0)]$ when the desired attenuation is reached. The density profile $n(r, z)$ was obtained by using $n(r, z)T(r, z) = P[Q(0)]/k_B$, and then normalizing to that at constant temperature T_0 and equilibrium pressure $P(0)$ in the low power limit.

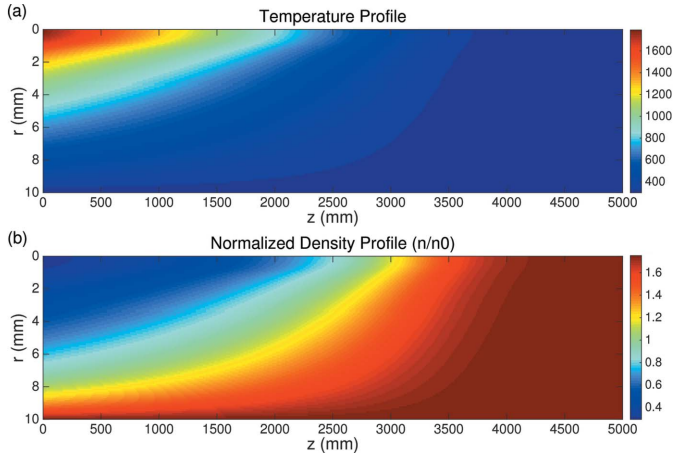

Figure 3
(a) The equilibrium temperature profile of the gas attenuator for attenuating by 10^5 a 200 eV soft X-ray FEL beam of 200 W average power. (b) The normalized density profile showing the ratio of the density distribution normalized to n_0, which is the density at the background temperature of 300 K if the input power is sufficiently small that the heating effect is completely negligible.

2.1.1. Equilibrium temperature and density distributions. Fig. 3(a) shows the equilibrium temperature profile $T(r, z)$ of the gas attenuator for attenuating by 10^5 a 200 eV soft X-ray FEL beam of 200 W CW average power. The simulation parameters were those specified in Fig. 2, and the pressure $P(0)$ in the low power limit was calculated to be 1.43 Torr. At the entrance of the attenuator $z \simeq 0$ and in the middle of the beam $r \simeq 0$, the temperature $T(0, 0)$ is elevated to $\sim$1800 K, nearly six times higher than the constant wall temperature of 300 K. $T(r, z)$ decreases both radially and along the z-axis towards the constant wall temperature as shown in Figs. 4(a) and 4(b). This temperature elevation rarefied the gas locally and led to the density depression or the so-called 'filamentation effect' starting at the entrance and extending both radially and in z as shown in Fig. 3(b), where the density profile was normalized by n_0, which is the density under the equilibrium pressure $P(0)$ in the low power limit and at the background temperature of T_0. The minimum density at $r \simeq 0$ and $z \simeq 0$ is only 30% of the low power limit, providing far less attenuation than required. As such, the equilibrium pressure $P[Q(0) =$ 200 W] must be raised from $P(0)$ of 1.43 Torr by as much as 75% to 2.51 Torr to compensate for the reduced attenuation in the front part of the attenuator, effectively 'jamming' 75% more gas particles in the back end of the attenuator to achieve the required attenuation. The axial and radial lineouts of the density profile are shown in Figs. 4(c) and 4(d).

The temperature profile, and thus the density profile and ultimately the achieved attenuation, has dependences on many parameters, including the geometry of the attenuator in diameter and in length, the CW input power, the size and profile of the FEL beam. Thus the exact achieved attenuation

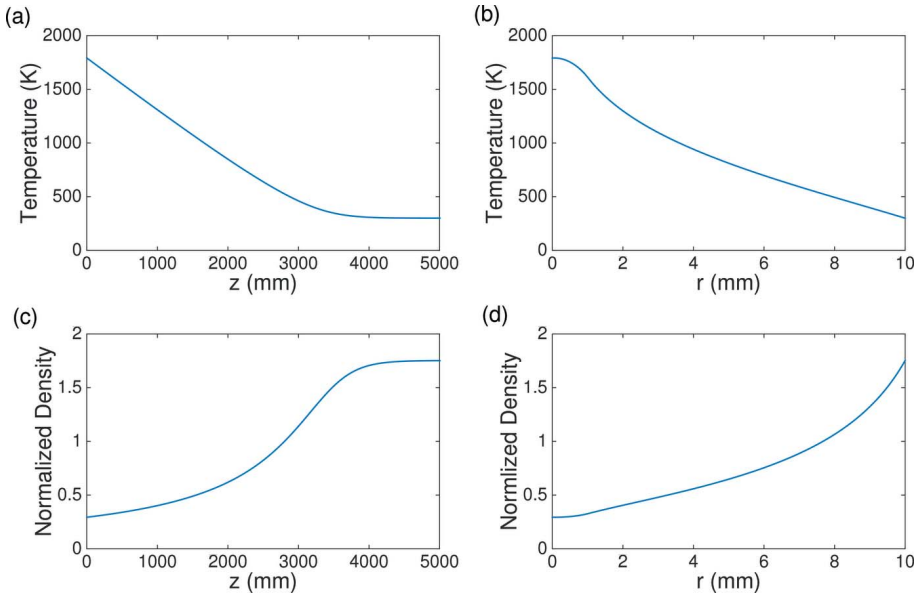

Figure 4
Lineouts from the two-dimensional profiles shown in Fig. 3. (*a*) The temperature profile along the *z*-axis at $r = 0$. (*b*) The temperature profile in the radial direction at $z = 0$. (*c*) The normalized density profile along the *z*-axis at $r = 0$. (*d*) The normalized density profile in the radial direction at $z = 0$.

could not be prescribed simply from knowing the attenuation length of the gas. However, in principle, a one-to-one relationship between the attenuation and the equilibrium pressure can be established first by simulation and then confirmed experimentally. In practice, this convoluted relationship presents operational challenges especially if the input power fluctuates on a time scale faster than the overall system relaxation time. This dynamic effect can only be revealed in a time-dependent simulation.

2.1.2. Dependences on input CW power. The filamentation effect stems from the continuing energy being injected into the gas system and the fact that the thermal conduction by the gas particles is finite. As the gas heats up, it expands, reducing its density. The rarefied gas absorbs less energy and reduces the heating. The heat is also being conducted away *via* thermal diffusion. Eventually the two processes reach a dynamic equilibrium when the absorbed energy is precisely offset by the energy loss through thermal conduction. As such, the filamentation effect is strongly dependent on the CW input power $Q(0)$ as shown in Fig. 5 for the required pressure, the maximum temperature and normalized density at the center of the entrance of the attenuator for a final achieved attenuation factor $\mu[Q(0)]$ of 10^5. The required pressure $P[Q(0)]$ asymptotically approaches the low power limit of 1.43 Torr as $Q(0) \rightarrow 0$, and the maximum temperature tends to the wall temperature of 300 K, and the normalized density to 1. It is clear that, in the case of the LCLS-I when the equivalent average power is less than 0.25 W, the filamentation or density depression effect is quite small and thus negligible. For a typical LCLS-II average power of 200 W and achieved attenuation of 10^5, the required pressure goes up to 2.51 Torr, the maximum temperature reaches 1800 K, and the normalized density goes to 0.3. At this power level, the behavior of the system is rather nonlinear due to the temperature-dependent thermal conductivity and the logarithmic dependence of equation (2) on the sizes of the FEL beam and the gas pipe. Fluctuations in the average FEL power will cause the effective attenuation to vary unpredictably if the pressure in the gas attenuation is regulated to a constant set point. This can be mitigated by measuring the actual FEL power after the attenuator if such a device itself is reliable, and the pressure can be put in a closed-loop control to achieve an average constant attenuation, although the response time of the system will be on milliseconds or longer time scales, making the pulse-to-pulse fluctuations impossible to tune out.

2.1.3. Dependences on attenuation factor. The dependences of the required pressure, maximum temperature and normalized density at the entrance of the attenuator on the desired attenuation were also mapped out at a constant input power of 200 W and are shown in Fig. 6. At an achieved attenuation of 10^5, the maximum temperature at the entrance of the attenuator reaches 1800 K, and the normalized density goes to 0.3, and the required pressure P(200 W) is raised to approximately 2.51 Torr. Even at low to moderate attenuation

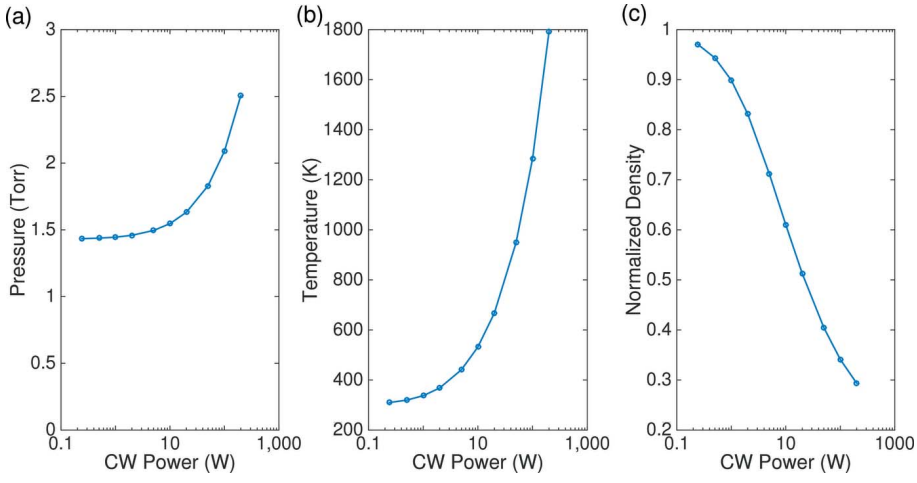

Figure 5
The dependence of (*a*) the required equilibrium pressure of the entire attenuator, (*b*) the maximum temperature at the central entrance of the attenuator and (*c*) the normalized density at the central entrance of the attenuator as a function of the CW input power for an actual achieved attenuation of 10^5.

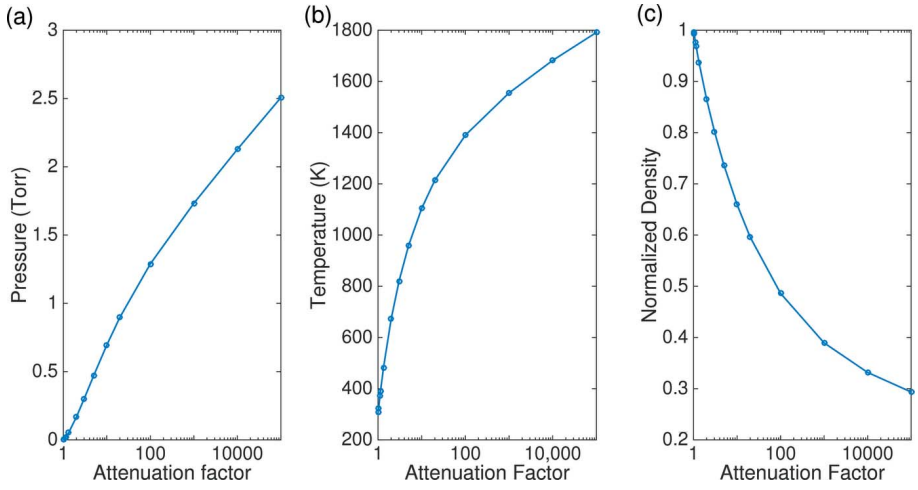

Figure 6
The dependence of (*a*) the required equilibrium pressure of the entire attenuator, (*b*) the maximum temperature at the central entrance of the attenuator, and (*c*) the normalized density at the central entrance of the attenuator as a function of the attenuation factor at a constant CW input power of 200 W.

levels, between a few to a few hundreds, the filamentation effect is still rather significant, as shown by the maximum temperature and the normalized density at the entrance of the gas pipe. The reason for this is that, even at an attenuation of 2, half of the FEL power or 100 W is dumped into the gas volume. In fact, the rate of change for all three parameters as a function of the attenuation factor is the greatest as it approaches 1. It is worth pointing out that this enhanced pressure sensitivity is problematic for gas-based detectors, and must be carefully studied and will be addressed separately. The potential issue in a gas-based system is that the deposited energy in the interaction volume as a result of producing a detectable signal is often comparable with the relevant energy scale of the gas particles; unless these gas particles have sufficient time to return to their original state or can be replaced reproducibly, the detectable signal will differ in level as well as in other aspects, thus rendering the intended measurement unreliable.

2.1.4. Effective attenuation. Because of the temperature/density gradient along the beam path, the FEL beam intensity does not vary exponentially as it would in the low power limit as shown in Fig. 7(*a*). In the front half of the attenuator the relative beam intensity decreases much slower, by roughly a factor of 3, than the low power limit indicated by the red dashed line, but in the back half it decreases much faster, by roughly 75%, as expected because of the stronger filamentation effect in the front half where the density drops to 30% of the low power limit while in the back half it is 75% higher. It is worth noting that, because of the dependence of the filamentation effect on intensity, the outer part of the beam where the intensity is lower will experience higher attenuation, causing the beam to self-focus. This effect can be clearly seen in Fig. 7(*b*), where the flat-top beam profile assumed initially at the entrance became more and more rounded as z increased. As such, the beam becomes effectively smaller, and thus is being self-focused. Self-focusing is an important effect for optical lasers (Askar'yan, 1962; Lallemand & Bloembergen, 1965) and has been studied extensively for many years.

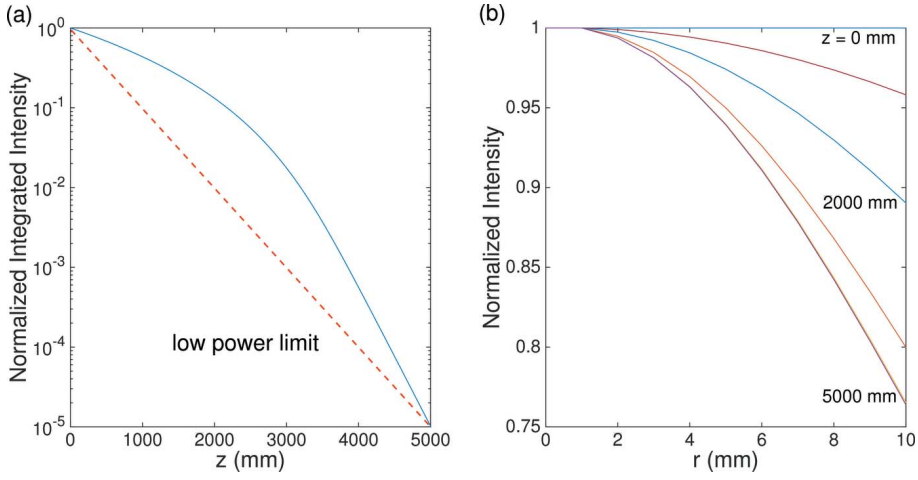

Figure 7
(*a*) The beam intensity in z along the attenuator at a constant CW input power of 200 W; the pressure was adjusted to make the final attenuation at 10^5. The dashed red line corresponds to the low power limit. (*b*) The self-focusing effect as shown by the changing beam profile from the initially assumed flat-top shape at z = 0 mm to be more rounded as z increases. The profiles at z = 4000 and 5000 mm are not distinguished due to the small differences as the self-focusing effect becomes small at lower beam intensities.

2.2. The transient solution for pulsed input of constant energy

For a pulsed FEL beam, the simulation for a CW input in §2 is not sufficient for understanding the time-dependent behavior of the system such as the effective attenuation, especially in terms of the impact of proceeding pulses on the trailing ones due to the filamentation effect. A simple examination of the system depicted in Fig. 2 filled with 1 Torr argon gas at room temperature indicates that its thermal relaxation time is of the order of a few milliseconds. As such, if the repetition rate of the FEL beam is greater than 1 kHz, the gas medium in the attenuator does not have sufficient time to relax completely back to its starting condition after each pulse. However, it is still possible for the system to establish a

'steady state' after many milliseconds if each pulse is identical such that the time-dependent behavior of the system simply repeats itself after each pulse. For example, the temperature at any given location is expected to rise and fall around the equilibrium temperature derived from the CW case, and the deviation depends on the repetition rate and the pulse energy. If, however, the pulse sequence has additional time scales in it, such as the macro pulse structure of the European XFEL beams, then the repetition of the system should also contain these exact time scales. The detail of the time-dependent simulation including the differential equation will not be presented here, but the result of a simple case, in which the FEL beam is operating at 100 kHz with 2 mJ per pulse and producing an equivalent power of 200 W, is shown in Fig. 8 and will be discussed.

The temperature at the entrance of the attenuator regulated to 2.51 Torr oscillates between a lower bound of ~1450 K and an upper bound of ~2370 K book-ending the equilibrium value of ~1800 K (red dashed line) obtained for the CW input case given by equation (2) and in Figs. 3 and 4(*a*). This is expected as the equilibrium temperature of the CW input represents the asymptotic temperature when the repetition rate is increased while reducing the per-pulse energy but keeping a 200 W constant average power. However, since any given trailing pulse 'sees' the lower bound temperature, it experiences a higher attenuation of 2.3×10^5 than that given by the CW input simulation at 1×10^5. As such, the dynamic value for the required pressure to achieve 10^5 attenuation should be slightly lower than 2.51 Torr.

If repeating the same simulation at half the repetition rate but twice the pulse energy, the system has 20 μs as opposed to 10 μs to relax from a higher temperature bound due to the higher per-pulse energy. The net change is indeed a lowering of the lower bound temperature and thus reducing the required pressure further. This is made possible by the virtue of the temperature dependence of the thermal conductivity of an ideal gas, which is proportional to $\sqrt{T}$. The situation may break down if the per-pulse energy is raised to the point where the assumptions made in this paper are no longer valid.

3. Concluding remarks

The effect of filamentation or density depression in a gas attenuator serving a high-repetition-rate X-ray FEL beam was shown and the degree of which it exhibited a complex relationship with many physical attributes of the system, including the gas species, pressure, input power, desired attenuation, and geometries of both the beam itself and the attenuator. As such, the simple and direct correspondence between the gas pressure and prescribed attenuation, often assumed for a sufficiently low repetition rate (thus necessarily low average power) FEL beam, breaks down. The actual attenuation received by any given pulse becomes a function of what came before, and for all intents and purposes is unpredictable given the nature of intensity fluctuations in SASE FEL pulses. The user must then rely on a pulse energy monitor downstream of the attenuator for more precise pulse energy information. A potential pitfall also exists for this mitigation strategy, since certainly in the case of soft X-rays the pulse energy monitor will be gas-based as well and the very same thermal effect is expected to impact the performance and precision of the energy measurement.

The fundamental issue with using a (low-temperature) gas medium for attenuation or energy measurement stems from the fact that the total energy of the gas particles in the kinetic degrees of freedom is too low compared with the amount of energy it is designed to absorb for either attenuation purpose or energy measurement. Under typical operating conditions, the total kinetic energy of all gas molecules ($\sim NkT \sim PV$) in the entire volume intercepted by the beam is often well below 1 mJ, which is roughly the average energy of the FEL pulses. On the intra-pulse time scale of 10 μs for a high-repetition-rate FEL beam of 100 kHz, the thermal diffusivity of the gas is sufficiently low that the diffusion length is of order 1 μm and

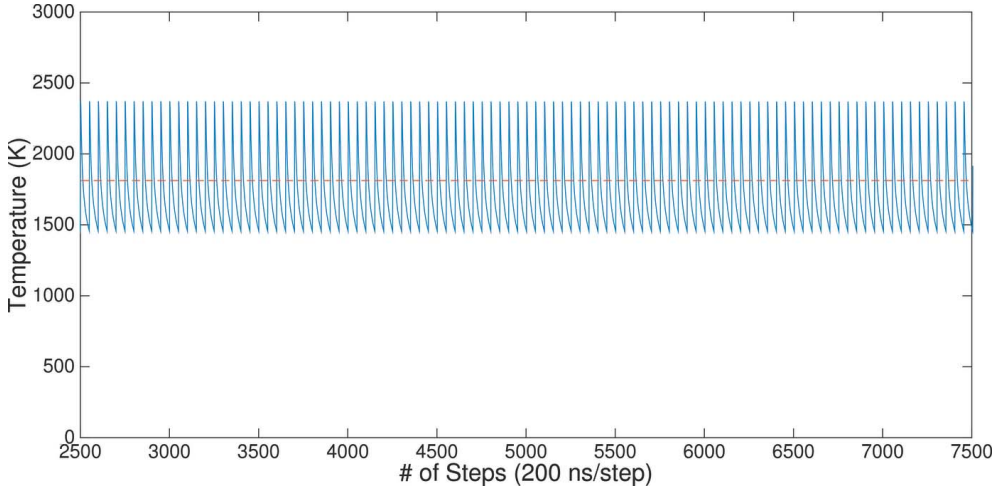

Figure 8
The time-dependent temperature at the entrance of the argon gas filled attenuator for a 100 kHz high-repetition-rate 200 eV soft X-ray FEL beam with 2 mJ per pulse. The pressure is regulated to 2.51 Torr. The red dashed line indicates the equilibrium temperature for a CW input of 200 W power. The intra-pulse time is 10 μs.

the absorbed energy stays relatively close to the beam, and does not disperse sufficiently far. Thus the gas heats up and then expands, lowering its density, which is responsible for attenuating the beam in the first place.

The results obtained in this study are predicated on the many assumptions being valid, such as the time scale of the pressure equilibration, and that thermal diffusion becomes the predominant mechanism for energy dissipation. There are of course other channels for the absorbed energy to escape the interaction volume, perhaps at faster time scales and in a more efficient manner. Further studies to understand the hydrodynamic and plasma-physics issues at shorter time scales of <1 µs are currently being carried out to validate these thermodynamic simulations.

There are possible mitigation mechanisms to minimize the filamentation effect. The size of the pipe could be optimized to allow more efficient cooling of the gas, and a longer gas volume would help as well by increasing the thermal contact of the gas volume with the cooling surfaces. To address the fundamental issue with the gas-based attenuator having too low an energy scale, one may envision a plasma-based attenuator system (Hershcovitch *et al.*, 2015) whose energy scale is much higher at a few eV or 10000 K. The operating power of a self-sustained plasma column can run as high as tens of kilowatts, much higher than the 200 W FEL power it would have to dissipate, and thus the input FEL power becomes a perturbation to the plasma system, which is an entirely different situation in a (cold) gas-based attenuator concept.

Acknowledgements

Use of the Linac Coherent Light Source (LCLS), SLAC National Accelerator Laboratory, is supported by the US Department of Energy, Office of Science, Office of Basic Energy Sciences under Contract No. DE-AC02-76SF00515.

References

Ackermann, W. *et al.* (2007). *Nat. Photon.* **1**, 336–342.
Allaria, E. *et al.* (2012). *Nat. Photon.* **6**, 699–704.
Askar'yan, G. A. (1962). *Soviet Phys. JETP*, **15**, 1088.
Cheng, Y.-H., Wahlstrand, J. K., Jhajj, N. & Milchberg, H. M. (2013). *Opt. Express*, **21**, 4740.
Emma, P. *et al.* (2010). *Nat. Photon.* **4**, 641–647.
Hahn, U. & Tiedtke, K. (2007). *AIP Conf. Proc.* **879**, 276–282.
Hershcovitch, A., Feng, Y., Fisher, A., Krzywinski, J. & Benwell, A. (2015). Private communication.
Ishikawa, I. *et al.* (2012). *Nat. Photon.* **6**, 540–544.
Lallemand, P. & Bloembergen, N. (1965). *Phys. Rev. Lett.* **15**, 1010–1012.
Ryutov, D. D. *et al.* (2009). Technical Report LLNL-TR-421318. Lawrence Livermore National Laboratory, Livermore, CA 94550, USA.
Schafer, D. W. (2015). Private communication.